Icarus 287 (2017) 131–139

Contents lists available at ScienceDirect

Icarus

journal homepage: www.elsevier.com/locate/icarus

Pluto–Charon solar wind interaction dynamics

J.P.M. Hale*, C.S. Paty

School of Earth and Atmospheric Sciences, Georgia Institute of Technology, Atlanta, GA 30332, United States

ARTICLE INFO

Article history:
Received 16 February 2016
Revised 16 November 2016
Accepted 29 November 2016
Available online 6 December 2016

Keywords:
Pluto
Charon
Solar wind
Ionospheres

ABSTRACT

This work studies Charon's effects on the Pluto-solar wind interaction using a multifluid MHD model which simulates the interactions of Pluto and Charon with the solar wind as well as with each other. Specifically, it investigates the ionospheric dynamics of a two body system in which either one or both bodies possess an ionosphere. Configurations in which Charon is directly upstream and directly downstream of Pluto are considered. Depending on ionospheric and solar wind conditions, Charon could periodically pass into the solar wind flow upstream of Pluto. The results of this study demonstrate that in these circumstances Charon modifies the upstream flow, both in the case in which Charon possesses an ionosphere, and in the case in which Charon is without an ionosphere. This modification amounts to a change in the gross structure of the interaction region when Charon possesses an ionosphere but is more localized when Charon lacks an ionosphere. Furthermore, evidence is shown that supports Charon acting to partially shield Pluto from the solar wind when it is upstream of Pluto, resulting in a decrease in ionospheric loss by Pluto.

1. Introduction

Pluto's discovery in 1930 was followed several decades later by that of its companion, Charon, in 1978. Here we will be exploring the role that Charon plays in the system's interaction with the solar wind as a result of the unique properties of the Pluto–Charon system, including those of Pluto's atmosphere. Following the confirmation of its existence through stellar occultation in 1989, Pluto's atmosphere has undergone notable and unexpected change. This consists of a large and sustained increase in estimated surface pressure, from ~ 5 μbar in 1988 (Elliot et al., 1989; Sicardy et al., 2003) to between 6.5 and 24 μbar in 2008 (Lellouch et al., 2009), with surface pressure at the time of the New Horizons encounter measured as ~ 10 μbar (Gladstone et al., 2016). This result was unexpected, as Pluto passed perihelion in 1989 and its atmosphere was therefore expected to be decreasing in surface pressure. Possible explanations for this include a change in albedo due to orbital orientation or changes in surface composition as well as thermal inertia (Elliot et al., 2003). It has long been suspected that Pluto's atmosphere freezes out completely as it approaches aphelion, however, recent simulations done by Olkin et al. (2015) suggest that this is not the case. Pluto's primary atmospheric constituent is N_2 but it also contains 0.25% CH_4 and trace amounts of higher hydrocarbons (Stern et al., 2015b). A thermal inversion is present through much of Pluto's lower atmosphere, the surface temperature being ~ 40 K and the peak atmospheric temperature approaching 100 K (Lellouch et al., 2009). Results from the New Horizons encounter also indicate that Pluto's atmosphere is more compact and slightly cooler than modeling based on stellar occultations had suggested (Gladstone et al., 2016; Stern et al., 2015b). This, in combination with a higher than anticipated solar wind density (Bagenal et al., 2016), resulted in the bow shock created by the interaction of the solar wind with Pluto's ionosphere being closer than expected at 4.5 Pluto radii upstream (McComas et al., 2016). Chemical modeling of Pluto's atmosphere indicates that ionospheric constituents consist of several distinct groups, centered at 1/28, 1/40, and 1/53 q/Da (elementary charge/dalton), the most abundant of which is 1/28 q/Da and is composed of $HCNH^+$ and $C_2H_5^+$ (Krasnopolsky and Cruikshank, 1999).

Charon is over half Pluto's radius (1 $R_P \approx 1187$ km and 1 $R_C \approx 606$ km (Stern et al., 2015b)), orbits 16.5 R_P from Pluto with a period of 6.4 days (Buie et al., 2006), and has a surface that is compositionally distinct from Pluto (almost exclusively H_2O in contrast to widespread N_2 and trace methane ices present on Pluto (Stern et al., 2015b), which are more volatile). Like Pluto (Cravens and Strobel, 2015), Charon is not expected to have an intrinsic magnetic field. This mixture of features results in a unique situation in which a moon might have a large impact on the solar wind interaction of its companion on a continuous basis. Additionally, there are several possible mechanisms that have been proposed through which

* Corresponding author.
E-mail addresses: john.p.m.hale@gatech.edu, john.p.m.hale@gmail.com (J.P.M. Hale).

http://dx.doi.org/10.1016/j.icarus.2016.11.036
0019-1035/© 2016 Published by Elsevier Inc.

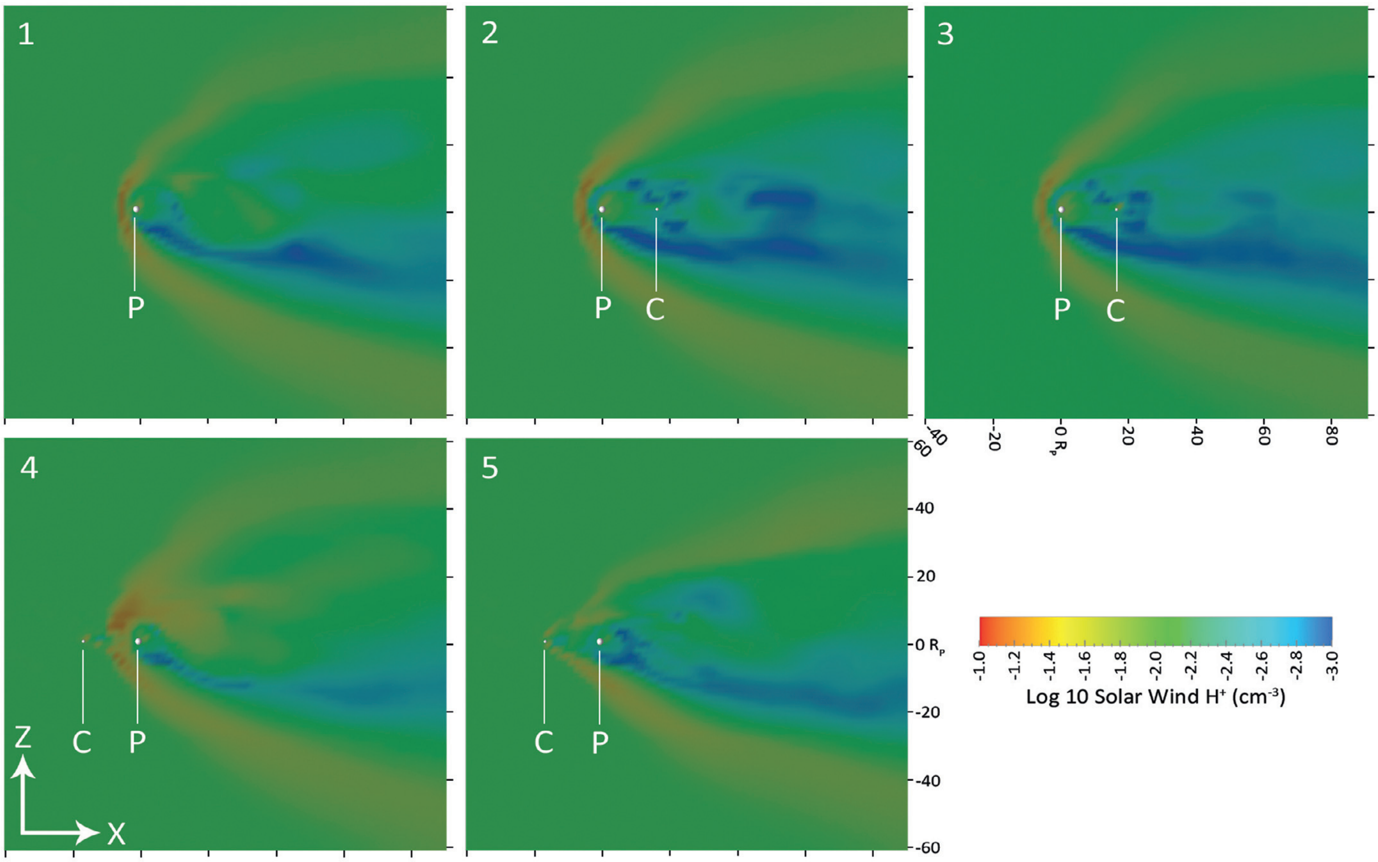

Fig. 1. Number density of H^+ from the solar wind for each test case is shown in the XZ plane (Y is pointing out of the plane). Solar wind flow is in the positive X direction and the IMF is pointed in the negative Y direction. Positions of Pluto and Charon are labeled in each case and each body is at Y = 0.

Table 1
Plasma parameters used for Solar Wind, Pluto, and Charon. *Temperatures are incorporated through the state equation. **Peak ion density for the Charon sourced species is not set to exactly 0 cm^{-3} due to numerical constraints.

Parameter	Value(s) Used
Magnetic field (nT)	0.2 (Bagenal et al., 1997)
Solar wind speed (km/s)	380 (Bagenal et al., 2015)
Solar wind density (cm^{-3})	0.01 (Bagenal et al., 1997)
Solar wind temperature (K)*	9000 (Richardson and Smith, 2003)
Pluto peak ion density (cm^{-3})	750 (Krasnopolsky and Cruikshank, 1999)
Pluto ion temperature (K)*	130 (Sicardy et al., 2003)
Charon peak ion density (cm^{-3})	25, ~ 0**
Charon ion temperature (K)*	40

Table 2
Simulations performed. All cases were run for 1500 s of simulated time in order to allow for a quasi-steady-state to be reached.

Charon absent	(1)	
Charon without Ionosphere	Charon downstream (2)	Charon upstream (4)
Charon with Ionosphere	Charon downstream (3)	Charon upstream (5)

Charon could at times possess a trace atmosphere and therefore ionosphere. These include a water group atmosphere sourced from cryovolcanism (Cook et al., 2007), a parasitic N_2 atmosphere derived from material escaping from Pluto (Tucker et al., 2015), and a transient, impact-sourced atmosphere (Stern et al., 2015a). The average age of Charon's surface (Moore et al., 2016) makes it unlikely that cryovolcanism has recently occurred on Charon. Similarly, measurements by the Alice UV spectrometer aboard New Horizons appear to preclude Charon currently possessing an atmosphere (Gladstone et al., 2016). However, the craters which appear to rule out recent cryovolcanic activity on Charon reaffirm that large impactors periodically hit Charon, demonstrating that Charon must go through phases of possessing an ionosphere (Stern et al., 2015a). This means that, during these periods in which Charon possesses an ionosphere, an ion source distinct from that of Pluto is moving through the Pluto system. In addition to this, the presence of an ionosphere around Charon must appreciably increase any alteration or obstruction of plasma flows within the system that are caused by Charon. While in the freestream upstream of Pluto – as the compact Plutonian atmosphere reported by Gladstone et al. (2016) suggests that Charon is for much of its orbit – Charon is likely to significantly modify conditions of the flow incident upon Pluto's ionosphere. This possibility is intriguing, as, while many moons locally alter the shock of their parent bodies while crossing the shock (Nishino et al., 2011), the only similar occurrence in which the moon was directly upstream of the parent body that has been observed within the solar system was during Cassini's T96 flyby of Titan, when Titan was determined to be outside of Saturn's bow shock (Bertucci et al., 2015). However, Charon's large size relative to Pluto compared to Titan's relative to Saturn indicates that any effect would be more significant on a global scale. A plausible result of this is that Charon could cause a decrease in atmospheric loss from Pluto through shielding from the solar wind. Another possible effect of Charon on Pluto's plasma environment is the modification of Pluto's plasma wake structure. This could be due to either physical obstruction by Charon itself or by the introduction of plasma into the region.

Previous work on the Pluto-solar wind interaction performed by Delamere has focused on instabilities using a 3D hybrid model (Delamere, 2004, 2009), while work by Harnett has compared

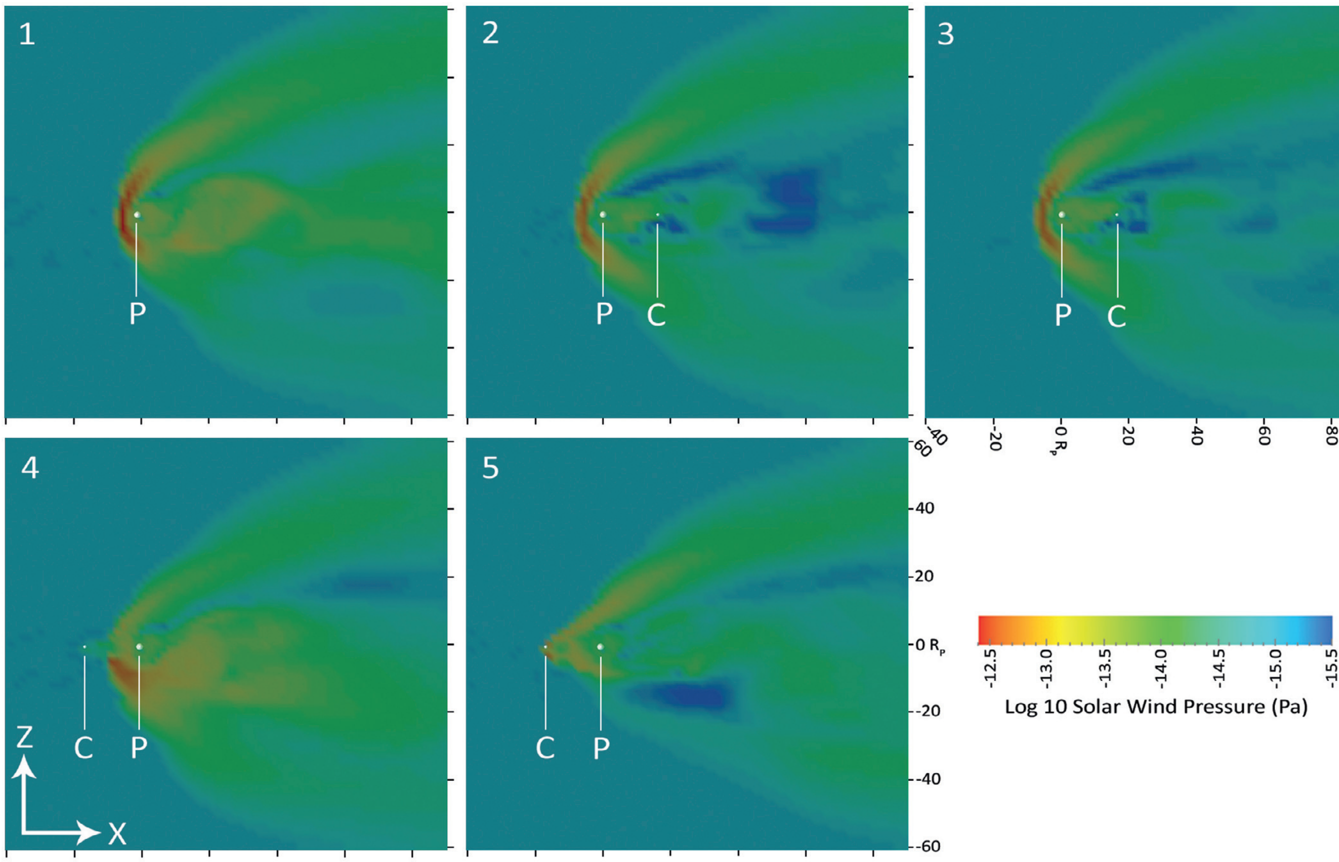

Fig. 2. Solar wind H^+ plasma pressure for each test case is shown in the XZ plane. Frames are oriented as in Fig. 1.

results using the Delamere hybrid model with results from a model derived from a 3D multifluid MHD model (Winglee, 1998; Harnett et al., 2005). Charon's presence within the system was not considered in these previous studies and therefore no simulations of the system which account for Charon have been performed. In contrast, this work is concerned with Charon's effects on the Plutonian interaction with the solar wind, with particular emphasis placed on any impact that Charon, while upstream of Pluto, may have on the formation of a bow shock in the system. Both system geometry and the presence of an ionosphere around Charon are considered in different scenarios simulated for the present work.

2. Model

The model that was used in this study is an evolved form of a multifluid treatment that has been applied to numerous planetary bodies in the past. Previously studied bodies include Ganymede (Paty and Winglee, 2006) and Titan (Snowden et al., 2011), as well as the study at Pluto which compared results from hybrid and multifluid MHD models (Harnett et al., 2005). The model is a global, three-dimensional, fully multifluid, magnetohydrodynamic model, which is appropriate for the Pluto system as the freestream turning distance of solar wind H^+ ($\sim$ 17 R_P) is smaller than the interaction region (defined as the diameter of the main shock on the plane passing through Pluto's terminator, which is > 35 R_P under simulated conditions), and the gyroradius of the solar wind H^+ within the shock and wake falls to as low as 1 R_P. It describes plasma behavior using a system of conservation equations, which are solved for each ion species: conservation of mass, conservation of momentum, and the equation of state. Electrons are treated as a separate, massless fluid where number density is derived through quasi-neutrality. Magnetic fields, electric fields, and currents are calculated using Maxwell's equations and the generalized Ohm's law. A second order Runge–Kutta method is used to solve each equation at each point on a nested grid.

In tracking several ion species, the conserved quantities are calculated separately for each ion species; here subscript α denotes the species, and subscript e the electrons, o indicates the planetary body, $\vec{v}$ is ion/electron velocity, P denotes pressure, q is ion charge, m is the mass, n is number density, ρ is mass density, and γ is the ratio of specific heats (set to 5/3 for this 3D simulation). $\vec{E}$ and $\vec{B}$ are the electric and magnetic fields, respectively, and $\vec{J}$ is the current density.

The conservation of mass (1), conservation of momentum (2), and time dependent pressure from equations of state pressure Eqs. (3) and (4) are from the multifluid formulation of Paty and Winglee (2006). The conservation of momentum equation has been modified to include a summation of gravitational terms, as shown in the braced term in Eq. (2)

$$\frac{\partial \rho_\alpha}{\partial t} + \nabla \cdot (\rho_\alpha \vec{v}_\alpha) = 0 \tag{1}$$

$$\rho_\alpha \frac{d\vec{v}_\alpha}{dt} = n_\alpha q_\alpha (\vec{E} + \vec{v}_\alpha \times \vec{B}) - \nabla P_\alpha - \left\{ \Sigma_o \left(\frac{GM_o}{R_o^2} \right) \rho_\alpha \hat{r}_o \right\} \tag{2}$$

$$\frac{\partial P_\alpha}{\partial t} = -\gamma \nabla \cdot (P_\alpha \vec{v}_\alpha) + (\gamma - 1)\vec{v}_\alpha \cdot \nabla P_\alpha \tag{3}$$

$$\frac{\partial P_e}{\partial t} = -\gamma \nabla \cdot (P_e \vec{v}_e) + (\gamma - 1)\vec{v}_e \cdot \nabla P_e \tag{4}$$

where M_o refers to the mass of the body in question and R_o refers to the distance between the particle and that body. An electron momentum equation, similar in form to Eq. (2), can be solved for

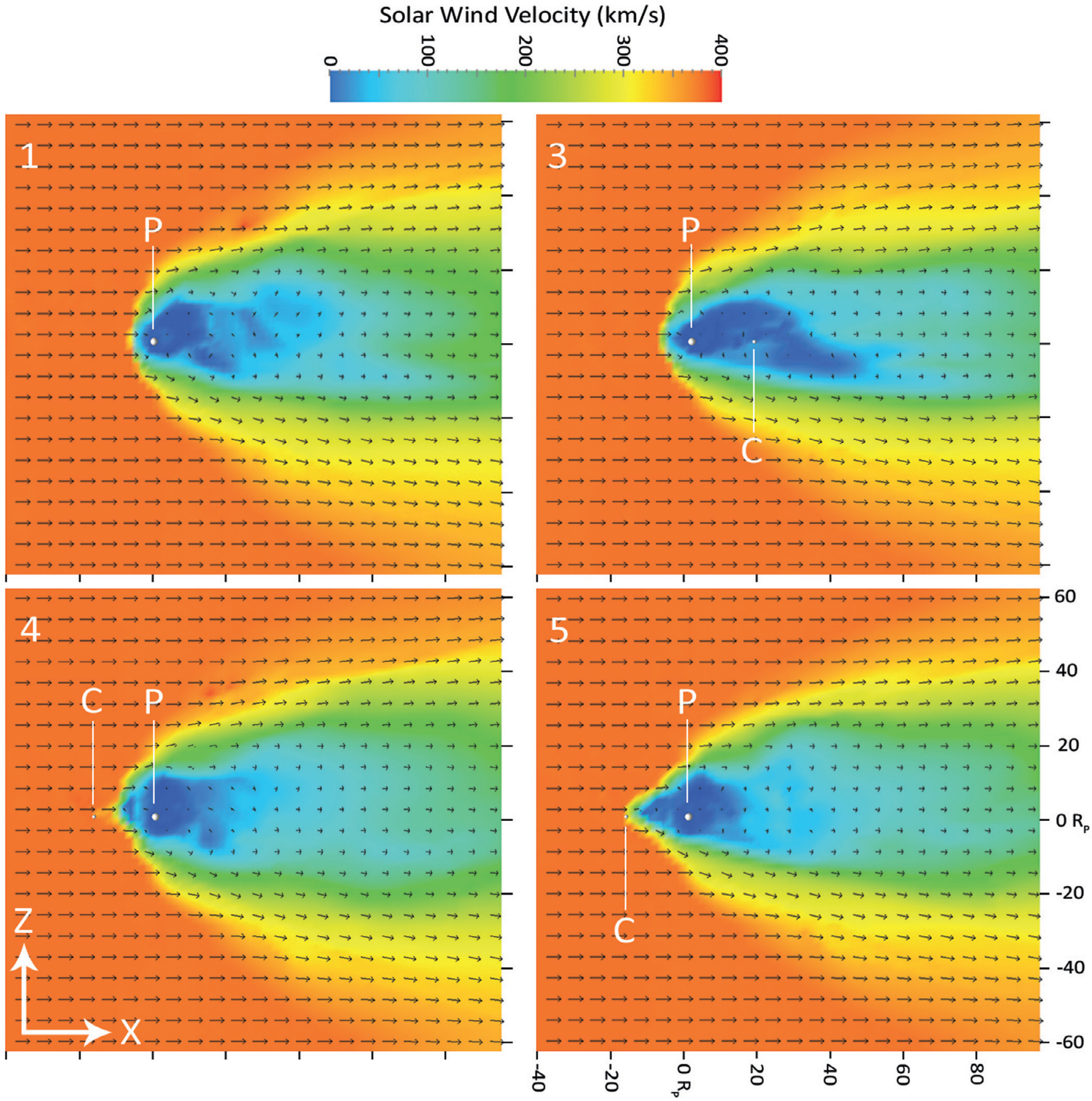

Fig. 3. Solar wind H$^+$ velocity vector fields are shown in the XZ plane for cases 1, 3, 4, and 5. Frames are oriented as in Fig. 1.

the electric field in the limit where $\frac{d\vec{v}_e}{dt}$ is small – a reasonable assumption given the ion cyclotron timescales present in this simulation (5–50 s) – and the gravity term is neglected in order to obtain a generalized Ohm's law. Since there are no large scale and rapidly changing electric fields we can assume a negligible displacement current, hence the plasma current, $\vec{J}$, can be described simply by:

$$\vec{J} = e(\Sigma_\alpha n_\alpha \vec{v}_e - n_e \vec{v}_e) \tag{5}$$

Eq. (5) can be solved for the electron velocity, $\vec{v}_e$, and substituted into Ohm's law to obtain a relationship independent of electron velocity.

$$\vec{E} = -\Sigma_\alpha \frac{n_\alpha \vec{v}_\alpha \times \vec{B}}{n_e} + \frac{\vec{J} \times \vec{B}}{en_e} - \frac{\nabla P_e}{en_e} + \eta(\hat{r})\vec{J} \tag{6}$$

Here the resistivity, η, is prescribed only at the base of the ionosphere of each object ($\sim 10^3$ ohm-meters); everywhere else in the simulation it is assumed to be zero. The changes in the magnetic field are determined by the induction equation below (7), which are then used with Ampère's Law (8) to find the associated currents.

$$\frac{\partial \vec{B}}{\partial t} = -\nabla \times \vec{E} \tag{7}$$

$$\vec{J} = \frac{1}{\mu_0} \nabla \times \vec{B} \tag{8}$$

These equations are solved explicitly at each grid point in a nested grid with second order accuracy. Charon is within the highest resolution box with a resolution of 64 km per grid point, while

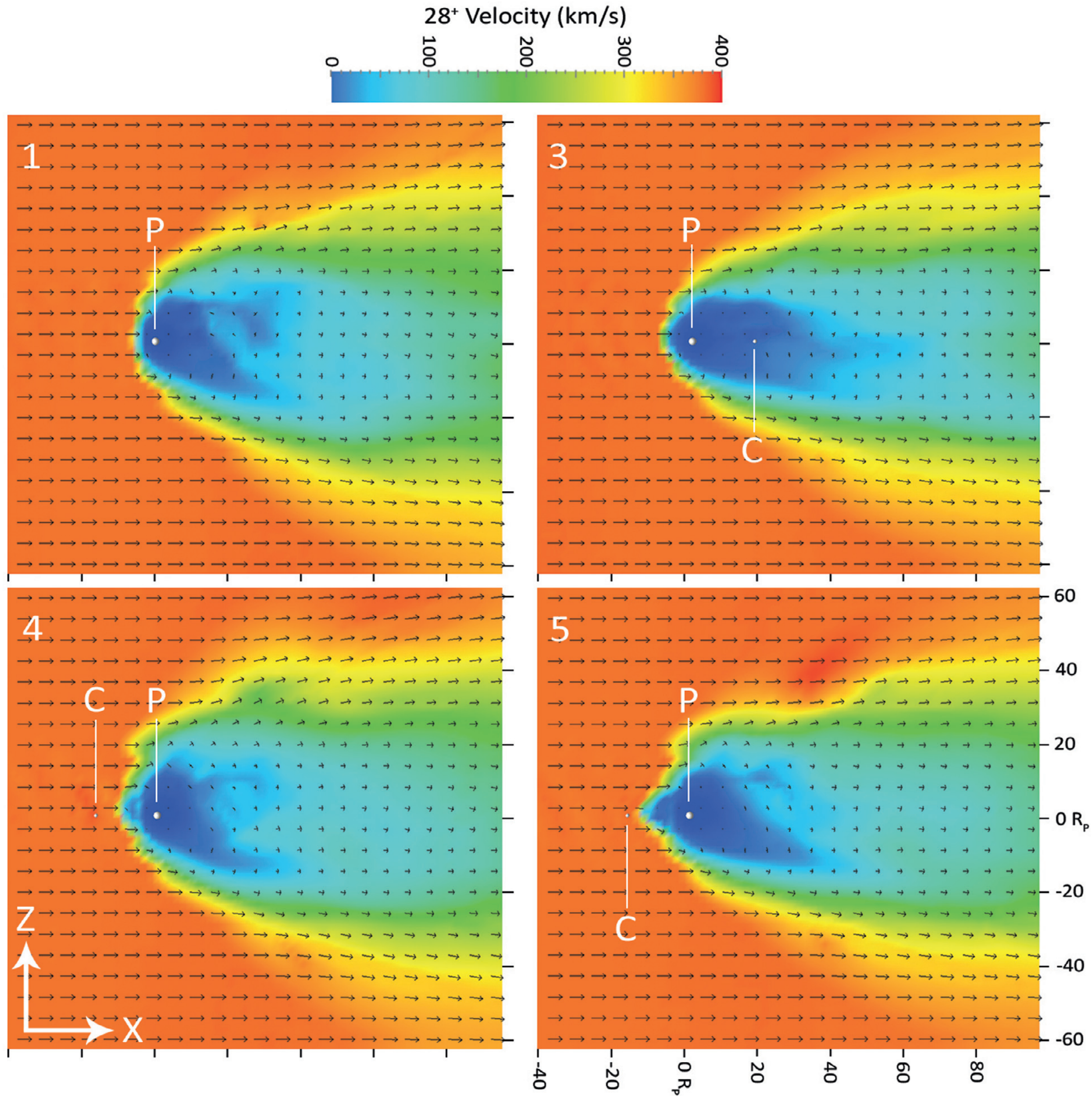

Fig. 4. Pluto sourced 28^+ velocity vector fields are shown in the XZ plane for cases 1, 3, 4, and 5. Velocities upstream of the shock correspond to numerically necessary trace amounts of Pluto sourced 28^+, as can be seen in Fig. 7. Deflection of velocity vectors on the -Z side of the wake demonstrates the presence of pickup ions, also as seen in Fig. 7. Frames are oriented as in Fig. 1.

Pluto is placed within the second box with a 128 km resolution. Total system size is 383 R_P in the X dimension and 125 R_P in Y and Z dimensions (455,00 km × 148,000 km × 148,000 km) where X is away from the Sun, Y is in the orbital direction, and Z completes the system. Ionospheric constituents are initialized based on a Chapman profile for the 1/28 q/Da group derived from the chemical modeling done by Krasnopolsky and Cruikshank (1999) using the parameters given in Table 1, combined with N_2^+ ionized in situ in the extended atmosphere. These populations are treated as one species, hereafter referred to as either Pluto sourced 28^+ or Charon sourced 28^+. Any ions that impact the surface of the bodies are assumed to be lost to the system.

The model has been enhanced in order to accommodate an arbitrary number of bodies within the simulation domain. Each body can be assigned a unique ionospheric structure and composition, magnetic field configuration, location, and other properties as required by the system under study. This allowed for the wide parameter space specified by this work to be explored efficiently.

A multifluid treatment is useful for this system as it allows for tracking of separate ion species. This is necessary as scenarios are considered in which Charon acts as a distinct ion source within the system. Additionally, the multifluid treatment is able to capture asymmetries within bow shocks that result from gyromotion of heavy pick up ions sourced from Pluto or Charon. The three fluid species used is this work are a solar wind H^+ species, a Pluto sourced 28^+ species, and – in cases 3 and 5 – a Charon sourced 28^+ species.

A series of simulations were run in order to characterize the behavior of the system throughout the relevant parameter space. System input parameters are shown in Table 1. These values were chosen in order to simulate what are expected to be typical solar wind and IMF conditions at Pluto, based on available data and

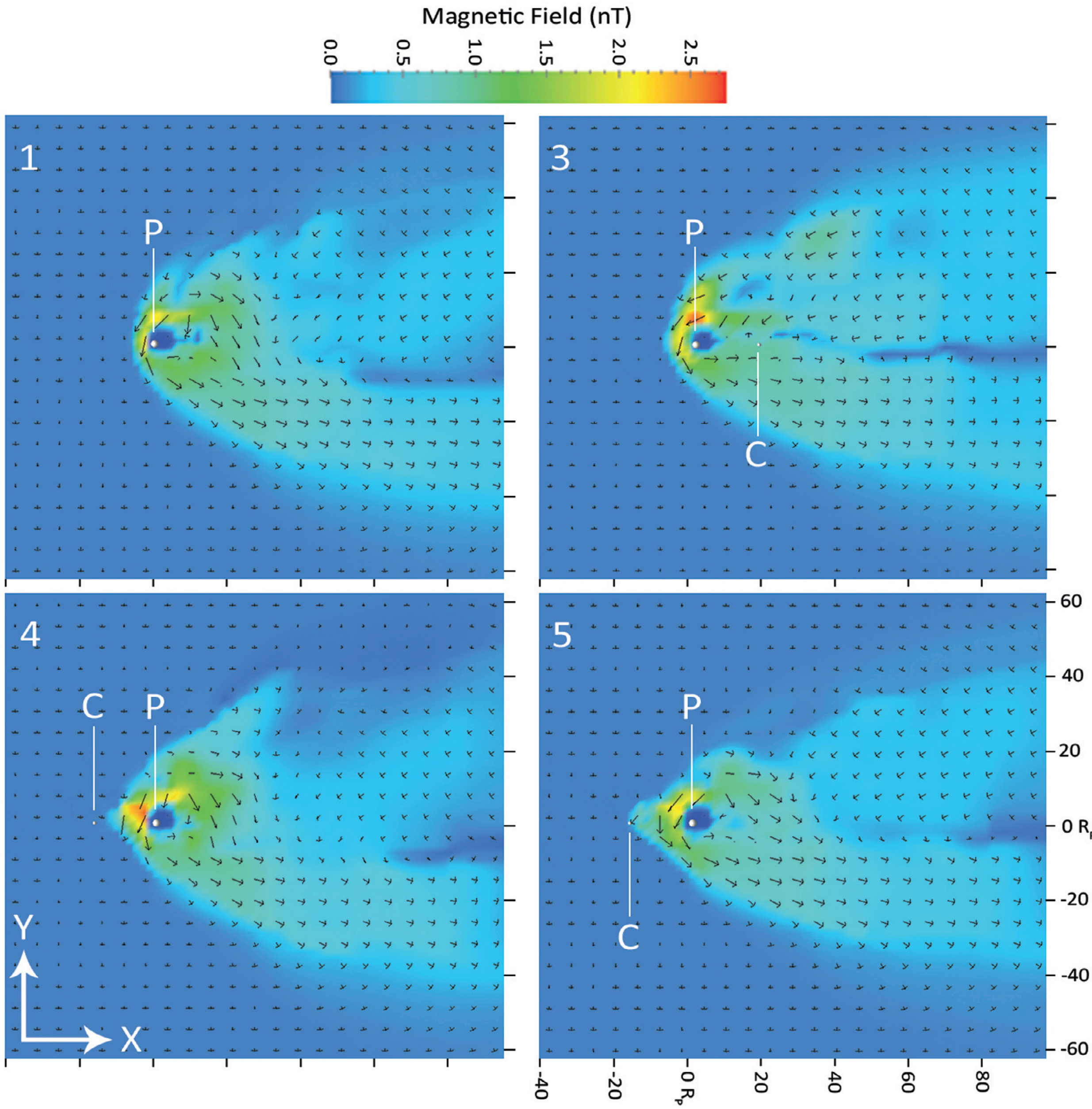

Fig. 5. Magnetic field vector fields are shown in the XY plane for cases 1, 3, 4, and 5 (Z is pointing into the plane). Solar wind flow is in the positive X direction. Positions of Pluto and Charon are labeled in each case and each body is at Z = 0.

modeling. Peak ionospheric number density at Pluto was based on chemical modeling performed by Krasnopolsky and Cruikshank (1999), while peak ionospheric density at Charon was chosen to be a small fraction of that at Pluto (3%) on the basis that any transient atmosphere which Charon may posses would be unlikely to be dense relative to Pluto's.

The primary parameters that were varied were the presence and location of Charon as well as the presence of an ionosphere around Charon, as shown in Table 2. These configurations were chosen in order to test the extremes of possible values for system parameters, as well as to generate a baseline for comparison in the instance of case 1. For context, Charon had no detectable ionosphere (Gladstone et al., 2016) and was to the side and slightly upstream of Pluto at the time of the New Horizons encounter. It was predicted that case 5 would exhibit the most extreme alteration due to the presence of Charon within the system.

3. Results

When Pluto is considered independently of Charon, as it is in case 1, the interaction between Pluto's ionosphere and the solar wind is what one would expect from an unmagnetized body. The subsolar standoff distance for the shock is at 7 R_P and the shock distance on the plane of the terminator is 20 R_P in the -Z direction and 15 R_P in the Z direction, in line with results from Harnett et al. (2005) with similar system parameters. Furthermore, a plasma sheet forms downstream of Pluto with corresponding draping of magnetic field lines, which is expected for such an obstacle to the flow of the solar wind. As can be seen by comparing cases 1 and 5 in Figs. 1 and 2, the shock structure sunward of Pluto is greatly altered by the presence of Charon upstream when Charon possesses an ionosphere. The maximum density enhancement decreases by $\sim$ 50% between cases 1 and 5 (in case 1 the H^+ density jumps from 0.01 cm^{-3} to 0.1 cm^{-3}, while in case

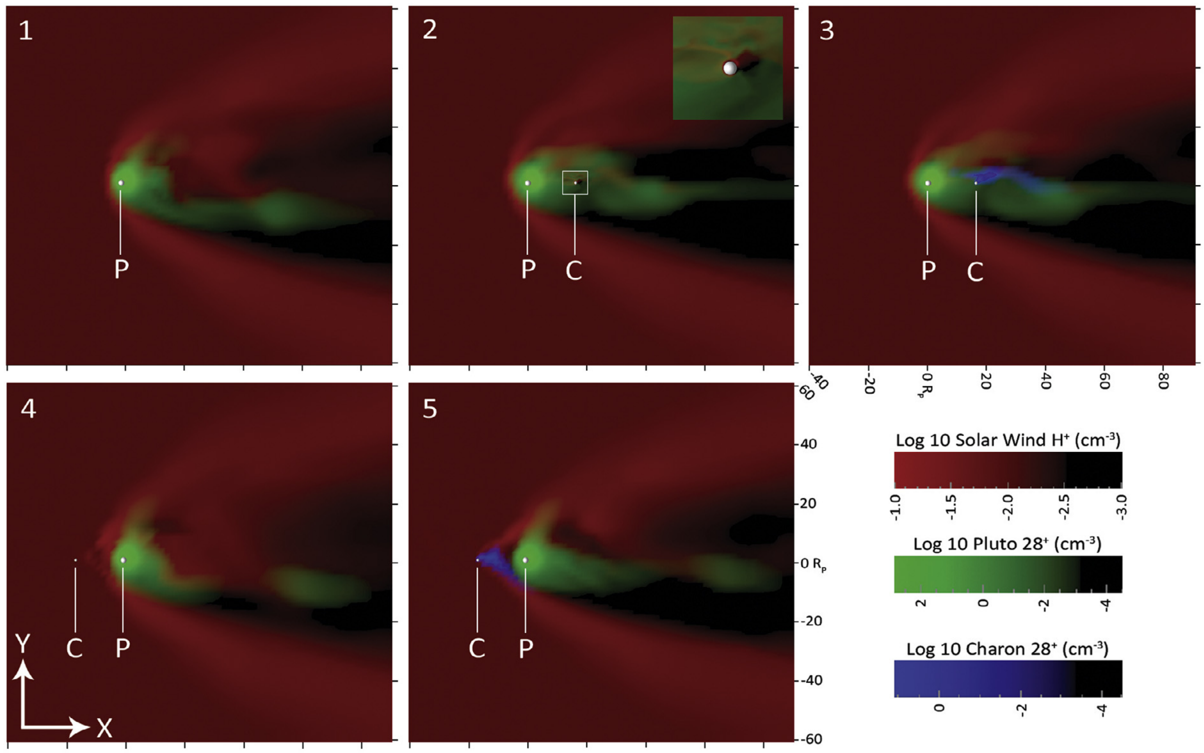

Fig. 6. Densities for each species are shown in the XY plane for all cases. Colors correspond to different species, with opacity indicating density. Red is solar wind H^+, green is 28^+ sourced from Pluto, and blue is 28^+ sourced from Charon. The magnified view of Charon in case 2 uses data from a higher resolution inner grid box in order to show the geometric wake downstream of Charon. This higher resolution data is also shown within the white indicator box. While a similar wake is present in case 3, no magnified view is provided, as the Charon sourced 28^+ ion species dominates the region in question. Frames are oriented as in Fig. 5. (For interpretation of the references to color in this figure legend, the reader is referred to the web version of this article.)

5 it only increases to 0.05 cm^{-3}) and the maximum plasma pressure within the shock drops by ~ 60% (from 600 fPa to 230 fPa). Furthermore, the region directly upstream of Pluto is at or below the freestream solar wind density. Additionally, the shock angle is decreased for the shock overall. While cases 2 and 3 demonstrate notable differences from case 1, namely more fine scale structure within the ionopause, they are largely similar to each other. Therefore only case 3 will be given attention in subsequent comparisons. As is to be expected given the supersonic, super-Alfvénic upstream conditions in case 4, the case in which Charon is upstream of Pluto but does not have an ionosphere, Charon causes a significant – if localized – effect. This is in contrast to the subsonic regimes that icy moons of Jupiter and Saturn typically inhabit.

The alterations to the structure of the interaction region in case 5 that were previously discussed are even more evident in the solar wind velocity fields shown in Fig. 3. Rather than the rounded shape seen in the upstream direction in cases 1 and 3, Pluto and Charon form a unified obstacle to the solar wind flow in case 5. Conversely, the confined nature of Charon's effect in case 4 is highlighted by looking at the velocity field. Asymmetries due to direction of the IMF dictating gyromotion are present in each of the cases, although they are most apparent in case 5 due to asymmetric pickup occurring from two distinct plasma sources as seen in Fig. 7.5. Magnetic field vector fields for each case are shown in Fig. 5. Charon's effects are less apparent in the magnetic field data than in the solar wind density and velocity data. While density increases are impeded and flow is drastically slowed by the presence of Charon, marked magnetic field increases are still present in the region between Pluto and Charon in case 5, with a lesser increase in the vicinity of Charon. Charon's effect on the magnetic field configuration is even less pronounced in case 4. Case 3 manifests a notable reconfiguration of magnetic fields relative to case 1. In case 3, the formation of the region of anti-parallel magnetic field lines, corresponding to a plasma sheet, behind Pluto is observed to occur closer in than in the other cases.

The density structure of these plasma sheets can be seen in Fig. 6. In case 3 of the figure, plasma originating from Charon is present in a region which is depleted of solar wind plasma. In each of the cases a concentration of solar wind H^+ predictably coincides with a region of anti-parallel magnetic field vectors shown in Fig. 5, indicating the location of the plasma sheet. A geometric wake in the flow of Pluto sourced 28^+ that extends ~ 3 R_C is present downstream of Charon in cases 2 and 3, as can be seen in Figs. 6 and 7. The IMF-caused asymmetries first mentioned in relation to Fig. 3 are far more obvious in the multispecies density plots shown in Fig. 7 as well as the plots of Pluto sourced 28^+ velocity vector fields displayed in Fig. 4. Both Pluto sourced 28^+ and Charon sourced 28^+ move preferentially in the -Z direction due to gryomotion. In case 1 the Pluto sourced pickup ions, as can be seen in Fig. 4, have a bulk velocity and density of ~ 100 km/s and 0.006 cm^{-3} respectively, which agrees well with measurements made by SWAP (Solar Wind Around Pluto) during the New Horizons encounter (90 km/s and 0.009 cm^{-3}) (McComas et al., 2016). As the ions move away from their parent bodies and into the magnetosheath, they follow the direction on the magnetic field within the magnetosheath. This is to be expected, as the ions only undergo gyromotion if their velocity vector has a component which is perpendicular to the direction of the magnetic field through which they are traveling. In cases 1 and 3, in which the shock structure is not altered by Charon, the gyromotion of heavy pick up ions from Pluto is less subtle than in case 4, which is in turn less subtle than in case 5. This is a consequence of the shock angle

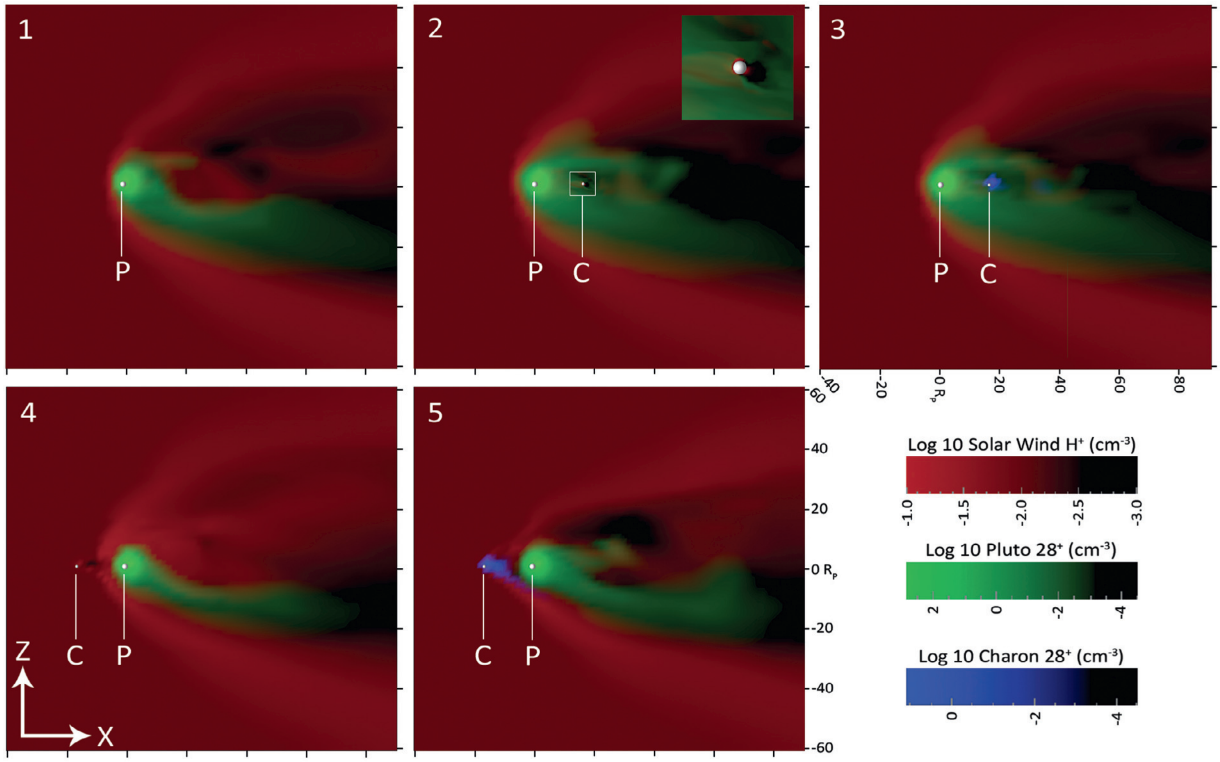

Fig. 7. Densities for each species are shown in the XZ plane for all cases. Colors correspond to different species, with opacity indicating density. Red is solar wind H^+, green is 28^+ sourced from Pluto, and blue is 28^+ sourced from Charon. The magnified view of Charon in case 2 uses data from a higher resolution inner grid box in order to show the geometric wake downstream of Charon. This higher resolution data is also shown within the white indicator box. While a similar wake is present in case 3, no magnified view is provided, as the Charon sourced 28^+ ion species dominates the region in question. Frames are oriented as in Fig. 1. (For interpretation of the references to color in this figure legend, the reader is referred to the web version of this article.)

and attendant shape of the magnetosheath. Close comparison of cases 4 and 5 against cases 1 and 3 in Figs. 4 and 5 reveals a 75% decrease ($\sim 5 \times 10^{-3}$ cm^{-3} vs. $\sim 2 \times 10^{-2}$ cm^{-3}) in peak density. We also calculated integrated fluxes of the Pluto sourced 28^+ species within the tail region 50 R_P downstream of Pluto, finding a flux of $\sim 1.11 \times 10^{24}$ s^{-1} in case 1, which is comparable to the $\sim 5 \times 10^{23}$ s^{-1} calculated by McComas et al. (2016) based on SWAP measurements made during the New Horizons encounter. For cases 4 and 5 we calculated fluxes of $\sim 9.2 \times 10^{23}$ s^{-1} and $\sim 9.0 \times 10^{23}$ s^{-1}, respectively. This corresponds to a 17% decrease in heavy ion flux between case 1 and case 4 and a 19% decrease between case 1 and case 5, suggesting that Charon is providing some degree of shielding against atmospheric loss while upstream.

4. Conclusions

The location of Charon within the system altered the interaction with the solar wind in several ways. In the case in which Charon has an ionosphere and is upstream of Pluto (case 5), the formation of a complete bow shock is prevented and the gross structure of the interaction between the solar wind and Pluto is clearly altered. Side effects of this alteration include changes to the trajectory of heavy pick up ions sourced from Pluto. The impact of Charon being upstream without an ionosphere (case 4) is less than with an ionosphere, but it is still non-negligible. Because Charon is mainly acting as a plasma absorber in this case, it can only have an effect as a result of several factors conspiring together: Charon's uniquely large size relative to the system it is in, its close orbital distance, supersonic, super-Alfvénic upstream flow, and Pluto's bow shock forming close to Pluto as a result of an atmosphere that is more compact than predicted. Both cases 4 and 5 show evidence for Charon shielding Pluto from atmospheric stripping while it is upstream of Pluto's bow shock. When Charon is downstream of Pluto, its impact on the system is more muted. With that said, in both the case of an ionosphere and the case of no ionosphere, Charon increases flow complexity in Pluto's wake and alters the path of the plasma sheet. Based on these results we expect the Pluto-Charon plasma environment to be highly dynamic independently of fluctuations in upstream solar wind conditions as a result of Charon's orbital motion.

SWAP measurements taken during the New Horizons encounter with the Pluto-Charon system indicate that solar wind density and, to a lesser extent, velocity were higher than predicted at 0.025 H^+/cm^3 (2.5× simulated value) and 403 km/s (1.06× simulated value) (Bagenal et al., 2016; McComas et al., 2009). This suggests that the bow shock at the time of the encounter would be more compressed than the results presented in this work indicate, but this is not expected to qualitatively change Charon's effects on the system. Encounter measurements also indicate that the dominant escaping species is not N_2 as was expected, but is rather CH_4 (Gladstone et al., 2016). Follow-up work is now underway in which Pluto and Charon are simulated in the orbital orientation that existed at the time of the encounter, CH_4^+ is the dominant ion species, and ion-neutral interactions are treated, creating dynamic volumetric plasma sources within the simulation domain. In addition to continuing to run cases using the expected average solar wind conditions, cases will be run with the heightened solar wind conditions measured during the encounter. This will allow for comparison against conditions for which results can be corroborated with data and provide greater assurance that results are reasonable and will also provide context for the limited available data.

Acknowledgment

This work was supported by NASA Grant NNX11AM40G, Georgia State Space Grant and the Georgia Institute of Technology. We would like to thank the reviewers for their valuable comments.

References

Bagenal, F., Cravens, T., Luhmann, J., McNutt, R., Cheng, A., 1997. Pluto's interaction with the solar wind. Pluto Charon 1, 523.

Bagenal, F., Delamere, P.A., Elliott, H.A., Hill, M.E., Lisse, C.M., McComas, D.J., McNutt Jr., R.L., Richardson, J.D., Smith, C.W., Strobel, D.F., 2015. Solar wind at 33 au: setting bounds on the pluto interaction for new horizons. J. Geophys. Res. 120 (9), 1497–1511. ISSN 2169-9100. doi: 10.1002/2015JE004880.

Bagenal, F., Horányi, M., McComas, D.J., McNutt, R.L., Elliott, H.A., Hill, M.E., Brown, L.E., Delamere, P.A., Kollmann, P., Krimigis, S.M., Kusterer, M., Lisse, C.M., Mitchell, D.G., Piquette, M., Poppe, A.R., Strobel, D.F., Szalay, J.R., Valek, P., Vandegriff, J., Weidner, S., Zirnstein, E.J., Stern, S.A., Ennico, K., Olkin, C.B., Weaver, H.A., Young, L.A., 2016. Pluto's interaction with its space environment: solar wind, energetic particles, and dust. Science 351 (6279). ISSN 0036-8075. doi: 10.1126/science.aad9045.

Bertucci, C., Hamilton, D., Kurth, W., Hospodarsky, G., Mitchell, D., Sergis, N., Edberg, N.J.T., Dougherty, M.K., 2015. Titan's interaction with the supersonic solar wind. Geophys. Res. Lett. 42 (2), 193–200. doi:10.1002/2014gl062106.

Buie, M.W., Grundy, W., Young, E., Young, L., Stern, S., 2006. Orbits and photometry of pluto's satellites: Charon, s/2005 p1, and s/2005 p2. Astron. J. 132 (1), 290. doi:10.1086/504422.

Cook, J., Desch, S.J., Roush, T., Trujillo, C., Geballe, T., 2007. Near-infrared spectroscopy of charon: possible evidence for cryovolcanism on kuiper belt objects. ApJ 663 (2), 1406–1419. doi:10.1086/518222.

Cravens, T., Strobel, D., 2015. Pluto's solar wind interaction: collisional effects. Icarus 246, 303–309. doi:10.1016/j.icarus.2014.04.011.

Delamere, P.A., 2004. Pluto's kinetic interaction with the solar wind. Geophys. Res. Lett. 31 (4). doi:10.1029/2003gl018122.

Delamere, P.A., 2009. Hybrid code simulations of the solar wind interaction with Pluto. J. Geophys. Res. 114 (A3). doi:10.1029/2008ja013756.

Elliot, J., Dunham, E., Bosh, A., Slivan, S., Young, L., Wasserman, L., Millis, R., 1989. Pluto's atmosphere. Icarus 77 (1), 148–170. doi:10.1016/0019-1035(89)90014-6.

Elliot, J.L., Ates, A., Babcock, B.A., Bosh, A.S., Buie, M.W., Clancy, K.B., Dunham, E.W., Eikenberry, S.S., Hall, D.T., Kern, S.D., Leggett, S.K., Levine, S.E., Moon, D.-S., Olkin, C.B., Osip, D.J., Pasachoff, J.M., Penprase, B.E., Person, M.J., Qu, S., Rayner, J.T., Roberts, L.C., Salyk, C.V., Souza, S.P., Stone, R.C., Taylor, B.W., Tholen, D.J., Thomas-Osip, J.E., Ticehurst, D.R., Wasserman, L.H., 2003. The recent expansion of Pluto's atmosphere. Nature 424 (6945), 165–168. doi:10.1038/nature01762.

Gladstone, G.R., Stern, S.A., Ennico, K., Olkin, C.B., Weaver, H.A., Young, L.A., Summers, M.E., Strobel, D.F., Hinson, D.P., Kammer, J.A., Parker, A.H., Steffl, A.J., Linscott, I.R., Parker, J.W., Cheng, A.F., Slater, D.C., Versteeg, M.H., Greathouse, T.K., Retherford, K.D., Throop, H., Cunningham, N.J., Woods, W.W., Singer, K.N., Tsang, C.C.C., Schindhelm, E., Lisse, C.M., Wong, M.L., Yung, Y.L., Zhu, X., Curdt, W., Lavvas, P., Young, E.F., Tyler, G.L., 2016. The atmosphere of pluto as observed by new horizons. Science 351 (6279). doi:10.1126/science.aad8866. ISSN 0036-8075

Harnett, E.M., Winglee, R.M., Delamere, P.A., 2005. Three-dimensional multi-fluid simulations of Pluto's magnetosphere: a comparison to 3d hybrid simulations. Geophys. Res. Lett. 32 (19), n/a–n/a. doi:10.1029/2005gl023178.

Krasnopolsky, V., Cruikshank, D., 1999. Photochemistry of Pluto's atmosphere and ionosphere near perihelion. J. Geophys. Res. 104 (E9), 21979–21996. doi:10.1029/1999je001038.

Lellouch, E., Sicardy, B., de Bergh, C., Käufl, H.-U., Kassi, S., Campargue, A., 2009. Pluto's lower atmosphere structure and methane abundance from high-resolution spectroscopy and stellar occultations. Astron. Astrophys. 495 (3), L17–L21. doi:10.1051/0004-6361/200911633.

McComas, D., Allegrini, F., Bagenal, F., Casey, P., Delamere, P., Demkee, D., Dunn, G., Elliott, H., Hanley, J., Johnson, K., Langle, J., Miller, G., Pope, S., Reno, M., Rodriguez, B., Schwadron, N., Valek, P., Weidner, S., 2009. The solar wind around Pluto (SWAP) instrument aboard new horizons. In: New Horizons. Springer Science Business Media, pp. 261–313.

McComas, D.J., Elliott, H.A., Weidner, S., Valek, P., Zirnstein, E.J., Bagenal, F., Delamere, P.A., Ebert, R.W., Funsten, H.O., Horanyi, M., McNutt, R.L., Moser, C., Schwadron, N.A., Strobel, D.F., Young, L.A., Ennico, K., Olkin, C.B., Stern, S.A., Weaver, H.A., 2016. Pluto's interaction with the solar wind. J. Geophys. Res. 121 (5), 4232–4246. ISSN 2169-9402. doi: 10.1002/2016JA022599.

Moore, J.M., McKinnon, W.B., Spencer, J.R., Howard, A.D., Schenk, P.M., Beyer, R.A., Nimmo, F., Singer, K.N., Umurhan, O.M., White, O.L., Stern, S.A., Ennico, K., Olkin, C.B., Weaver, H.A., Young, L.A., Binzel, R.P., Buie, M.W., Buratti, B.J., Cheng, A.F., Cruikshank, D.P., Grundy, W.M., Linscott, I.R., Reitsema, H.J., Reuter, D.C., Showalter, M.R., Bray, V.J., Chavez, C.L., Howett, C.J.A., Lauer, T.R., Lisse, C.M., Parker, A.H., Porter, S.B., Robbins, S.J., Runyon, K., Stryk, T., Throop, H.B., Tsang, C.C.C., Verbiscer, A.J., Zangari, A.M., Chaikin, A.L., Wilhelms, D.E., 2016. The geology of pluto and charon through the eyes of new horizons. Science 351 (6279), 1284–1293. doi:10.1126/science.aad7055. ISSN 0036-8075 URL http://science.sciencemag.org/content/351/6279/1284

Nishino, M.N., Wang, X.-D., Fujimoto, M., Tsunakawa, H., Saito, Y., Yokota, S., Bian, W., Li, C.-L., Matsushima, M., Shibuya, H., et al., 2011. Anomalous deformation of the earth's bow shock in the lunar wake: Joint measurement by chang'e-1 and selene. Planet. Space Sci. 59 (5), 378–386. http://dx.doi.org/10.1016/j.pss.2011.01.002.

Olkin, C., Young, L., Borncamp, D., Pickles, A., Sicardy, B., Assafin, M., Bianco, F., Buie, M., de Oliveira, A.D., Gillon, M., French, R., Gomes, A.R., Jehin, E., Morales, N., Opitom, C., Ortiz, J., Maury, A., Norbury, M., Braga-Ribas, F., Smith, R., Wasserman, L., Young, E., Zacharias, M., Zacharias, N., 2015. Evidence that Pluto's atmosphere does not collapse from occultations including the 2013 May 04 event. Icarus 246, 220–225. doi:10.1016/j.icarus.2014.03.026.

Paty, C., Winglee, R., 2006. The role of ion cyclotron motion at ganymede: magnetic field morphology and magnetospheric dynamics. Geophys. Res. Lett. 33 (10), n/a–n/a. doi:10.1029/2005gl025273.

Richardson, J., Smith, C., 2003. The radial temperature profile of the solar wind. Geophys. Res. Lett. 30 (5), n/a–n/a. doi:10.1029/2002gl016551.

Sicardy, B., Widemann, T., Lellouch, E., Veillet, C., Cuillandre, J.-C., Colas, F., Roques, F., Beisker, W., Kretlow, M., Lagrange, A.-M., Gendron, E., Lacombe, F., Lecacheux, J., Birnbaum, C., Fienga, A., Leyrat, C., Maury, A., Raynaud, E., Renner, S., Schultheis, M., Brooks, K., Delsanti, A., Hainaut, O.R., Gilmozzi, R., Lidman, C., Spyromilio, J., Rapaport, M., Rosenzweig, P., Naranjo, O., Porras, L., Díaz, F., Calderón, H., Carrillo, S., Carvajal, A., Recalde, E., Cavero, L.G., Montalvo, C., Barría, D., Campos, R., Duffard, R., Levato, H., 2003. Large changes in Pluto's atmosphere as revealed by recent stellar occultations. Nature 424 (6945), 168–170. doi:10.1038/nature01766.

Snowden, D., Winglee, R., Kidder, A., 2011. Titan at the edge: 1. Titan's interaction with Saturn's magnetosphere in the prenoon sector. J. Geophys. Res. 116 (A8). doi:10.1029/2011ja016435.

Stern, S., Gladstone, R., Zangari, A., Fleming, T., Goldstein, D., 2015a. Transient atmospheres on charon and water-ice covered KBOs resulting from comet impacts. Icarus 246, 298–302. doi:10.1016/j.icarus.2014.03.008.

Stern, S.A., Bagenal, F., Ennico, K., Gladstone, G.R., Grundy, W.M., McKinnon, W.B., Moore, J.M., Olkin, C.B., Spencer, J.R., Weaver, H.A., Young, L.A., Andert, T., Andrews, J., Banks, M., Bauer, B., Bauman, J., Barnouin, O.S., Bedini, P., Beisser, K., Beyer, R.A., Bhaskaran, S., Binzel, R.P., Birath, E., Bird, M., Bogan, D.J., Bowman, A., Bray, V.J., Brozovic, M., Bryan, C., Buckley, M.R., Buie, M.W., Buratti, B.J., Bushman, S.S., Calloway, A., Carcich, B., Cheng, A.F., Conard, S., Conrad, C.A., Cook, J.C., Cruikshank, D.P., Custodio, O.S., Ore, C.M.D., Deboy, C., Dischner, Z.J.B., Dumont, P., Earle, A.M., Elliott, H.A., Ercol, J., Ernst, C.M., Finley, T., Flanigan, S.H., Fountain, G., Freeze, M.J., Greathouse, T., Green, J.L., Guo, Y., Hahn, M., Hamilton, D.P., Hamilton, S.A., Hanley, J., Harch, A., Hart, H.M., Hersman, C.B., Hill, A., Hill, M.E., Hinson, D.P., Holdridge, M.E., Horanyi, M., Howard, A.D., Howett, C.J.A., Jackman, C., Jacobson, R.A., Jennings, D.E., Kammer, J.A., Kang, H.K., Kaufmann, D.E., Kollmann, P., Krimigis, S.M., Kusnierkiewicz, D., Lauer, T.R., Lee, J.E., Lindstrom, K.L., Linscott, I.R., Lisse, C.M., Lunsford, A.W., Mallder, V.A., Martin, N., McComas, D.J., McNutt, R.L., Mehoke, D., Mehoke, T., Melin, E.D., Mutchler, M., Nelson, D., Nimmo, F., Nunez, J.I., Ocampo, A., Owen, W.M., Paetzold, M., Page, B., Parker, A.H., Parker, J.W., Pelletier, F., Peterson, J., Pinkine, N., Piquette, M., Porter, S.B., Protopapa, S., Redfern, J., Reitsema, H.J., Reuter, D.C., Roberts, J.H., Robbins, S.J., Rogers, G., Rose, D., Runyon, K., Retherford, K.D., Ryschkewitsch, M.G., Schenk, P., Schindhelm, E., Sepan, B., Showalter, M.R., Singer, K.N., Soluri, M., Stanbridge, D., Steffl, A.J., Strobel, D.F., Stryk, T., Summers, M.E., Szalay, J.R., Tapley, M., Taylor, A., Taylor, H., Throop, H.B., Tsang, C.C.C., Tyler, G.L., Umurhan, O.M., Verbiscer, A.J., Versteeg, M.H., Vincent, M., Webbert, R., Weidner, S., Weigle, G.E., White, O.L., Whittenburg, K., Williams, B.G., Williams, K., Williams, S., Woods, W.W., Zangari, A.M., Zirnstein, E., 2015b. The Pluto system: initial results from its exploration by new horizons. Science 350 (6258). aad1815–aad1815. doi: 10.1126/science.aad1815.

Tucker, O., Johnson, R., Young, L., 2015. Gas transfer in the Pluto-Charon system: a charon atmosphere. Icarus 246, 291–297. doi:10.1016/j.icarus.2014.05.002.

Winglee, R.M., 1998. Multi-fluid simulations of the magnetosphere: the identification of the geopause and its variation with IMF. Geophys. Res. Lett. 25 (24), 4441–4444. doi:10.1029/1998gl900217.